

Self-Potential Observations During Hydraulic Fracturing in the Laboratory

Moore, Jeffrey R.

Glaser, Steven D.

University of California, Berkeley, 440 Davis Hall, Berkeley, CA, 94720, USA

Copyright 2005, ARMA, American Rock Mechanics Association

This paper was prepared for presentation at Alaska Rocks 2005, The 40th U.S. Symposium on Rock Mechanics (USRMS): Rock Mechanics for Energy, Mineral and Infrastructure Development in the Northern Regions, held in Anchorage, Alaska, June 25-29, 2005.

This paper was selected for presentation by a USRMS Program Committee following review of information contained in an abstract submitted earlier by the author(s). Contents of the paper, as presented, have not been reviewed by ARMA/USRMS and are subject to correction by the author(s). The material, as presented, does not necessarily reflect any position of USRMS, ARMA, their officers, or members. Electronic reproduction, distribution, or storage of any part of this paper for commercial purposes without the written consent of ARMA is prohibited. Permission to reproduce in print is restricted to an abstract of not more than 300 words; illustrations may not be copied. The abstract must contain conspicuous acknowledgement of where and by whom the paper was presented.

ABSTRACT: The self-potential (SP) response during hydraulic fracturing of an intact crystalline rock was investigated in the laboratory. Westerly granite cores were hydraulically fractured by applying water to the sample center at a constant rate. The SP response was monitored at 3 locations vertically on the sample perimeter, and the injection pressure was recorded. Results reveal a significant SP spike (up to 150 mV) at the time of failure, caused by the rapid migration of high pressure injectate into the newly created fracture void space. A system of micro-cracks was created in one test specimen by subjecting it to 9 cycles of heating and rapid quenching. The SP record for this sample indicated significant fluid infiltration prior to failure. This is in contrast to the 'fresh' specimen where little fluid flow was detected prior to failure, and indicates enhanced sample permeability due to dilatancy of micro-cracks. Finally, temporal resolution of the SP signals revealed the time of local fracture initiation and the direction of crack propagation. This testing demonstrates the ability of the SP method to respond to hydraulic fracture events, and may aid in both spatial and temporal monitoring of fracture networks in the field.

1. INTRODUCTION

The self-potential (SP) response during *compressional* loading of saturated intact rock specimens is well documented [1, 2, 3]. Researchers have noted an anomalous change in the SP response beginning at about 50-75% of the failure load. In related testing, electrical resistivity variations in rock samples have been characterized during frictional sliding and an anomalous decrease has been noted preceding failure [4, 5]. These results support the classical hypothesis that earth materials undergo dilatancy prior to failure, and local pore water diffuses into the low-pressure dilatant zone [6].

Mizutani et al. [7] first proposed that anomalous self-potentials may be created by migrating pore waters through electrokinetic coupling. Yoshida et al. [8] then demonstrated that there was no observable SP response during deformation in dry specimens, whereas there was a considerable SP

response for saturated basalt specimens. This provided evidence that observed electric self-potentials result from electrokinetic coupling.

We find little information, however, regarding the electrical response during *tensile* fracturing of earth materials, and even less regarding hydraulic fracturing. Wurmstich [9, 10] has shown numerical results proposing that the process of hydraulic fracturing augments the SP signal by up to an order of magnitude. He indicates that laboratory experiments were performed, but gives no references or results. Revil et al. [11] present analytical solutions for electrical anomalies created by thermohydromechanical disturbances in the context of hydrothermal circulation in an active volcanic system. They describe transient SP signals generated as hydraulic fracturing connects compartmentalized aquifers of varying fluid pressures and releases hydromechanical shock waves, demonstrating that significant surface anomalies can be expected. Finally, Kawakami and

Takasugi [12] and Marquis et al. [13] report surface SP data during hydraulic stimulation of hot dry rock reservoirs demonstrating good correlation between temporal SP variation and injection pressure and flow rate. Surface anomalies up to 40 mV are shown to correlate to both injection and flow-back events. Kawakami and Takasugi [12] also report the spatial surface SP variation, but do not mention the orientation of the induced fracture or if a correlation to fracture direction was evident. We have undertaken a research program to monitor the spatial and temporal SP response during hydraulic fracturing in the laboratory, and to decipher the origins these signals.

2. ELECTROKINETIC PHENOMENA

The laws controlling linear transport in porous media in the presence of electrokinetic coupling are [14]:

$$\mathbf{q} = -L_{11}\nabla p - L_{12}\nabla\phi \quad (1)$$

$$\mathbf{j} = -L_{21}\nabla p - L_{22}\nabla\phi \quad (2)$$

where \mathbf{q} is the volumetric fluid flow density, \mathbf{j} is the electric current density, p is the fluid pressure, and ϕ is the electric potential. When the double layer thickness is much smaller than a typical grain facet the transport coefficients are:

$$L_{11} = \frac{k}{\eta} \quad (3)$$

$$L_{12} = L_{21} = -\frac{\varepsilon\zeta}{\eta F} \quad (4)$$

$$L_{22} = \sigma_b \quad (5)$$

Here, k is the fluid-flow permeability, η is the dynamic fluid viscosity, ε is the dielectric constant of the fluid, σ_b is the bulk sample conductivity, F is the electrical formation factor, and ζ is the zeta potential, which is a measure of how much charge resides in the diffuse part of the electric double layer. The first term on the right-hand side of Equation (1) is Darcy's Law, the second term of Equation (2) is Ohm's Law, and the remaining terms represent the coupled electrokinetic effect with $L_{12} = L_{21}$ [15].

Electrokinetic phenomena arise from movement of ions in the electric double layer under a pore pressure gradient. Fluid flow causes mobile ions to be convected relative to the bound charge on the

mineral grain surfaces; charge motion known as the convection current. As this charge is deposited at the exit face of the sample and the bound charge is left exposed at the opposite face, a charge separation exists which drives an Ohmic return current, or the conduction current. In the absence of external current sources ($\mathbf{j} = 0$), the convection current ($L_{12}\nabla p$) and conduction current ($L_{22}\nabla\phi$) are equal and opposite, and equating them reveals the result of Smoluchowski [16]:

$$C_c = \frac{\Delta\phi}{\Delta p} = -\frac{L_{12}}{L_{22}} = \frac{\varepsilon\zeta}{\eta F \sigma_b} \quad (6)$$

where C_c is known as the streaming potential coupling coefficient.

3. EXPERIMENTAL

The test specimens were 57 mm diameter, 102 mm long cores of Westerly granite taken from the same block. A 6.35 mm diameter axial hole was drilled to within 25 mm of the bottom of each specimen. This hole was then over-cored at 9.53 mm diameter for 25 mm from the top of the sample to create a total vertical exposed bore length of 50 mm in the sample center. Next, the injector was prepared by machining a groove in 6.35 mm OD stainless steel tubing, which accepted a silicon o-ring. The injector was placed into the borehole so that the o-ring sat upon the lip created by the over-coring. Finally, the space around the steel tubing and above the o-ring was filled with a high-strength, non-conducting epoxy. The sample was then placed in an oven at 150°C for at least 12 hours to cure the epoxy and eliminate any pore fluid left over from drilling. Figure 1 illustrates the sample configuration.

Self-potentials were recorded on 3 electrodes spaced 25 mm vertically on the sample perimeter. The reference electrode for SP measurements was located on the bottom-center of each core (Figure 1). All electrodes were 13 mm square pieces of copper shim with a soldered jumper wire and were taped to the specimen perimeter. Voltage measurements were recorded at 500 samples per second for 128 second sweeps. Pressure measurements were recorded on an independent acquisition system at 4 samples per second.

The samples were wetted with water by placing them under vacuum and 2 m head for at least 48 hours. The pore fluid used for all testing was

0.001M NaCl solution ($\sigma_f = 0.013$ S/m, or $\rho_f = 77 \Omega\text{-m}$). Injectate was applied to the specimens at a constant rate of 0.154 ml/s via an injection pump. In each test, injection was begun 10 seconds after the start of data recording.

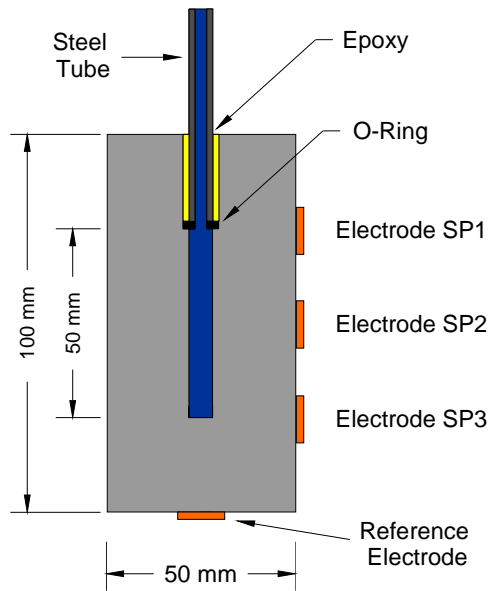


Fig. 1: Schematic of test specimens.

Prior to testing, specimen WG2 was subjected to 9 cycles of heating to 170°C and rapid quenching in 20°C water. This procedure was undertaken to create a system of micro-cracks in the sample lattice [17]. Specimen WG1 was left undisturbed and is therefore referred to as ‘fresh.’

4. RESULTS

Tensile fractures were induced in two Westerly granite cores by applying water at a constant rate to the sample center. There was no confining load on the specimens yet fracture geometry was consistent: axial and symmetric along the entire exposed length (50 mm) at the center. The specimen halves did not separate following fracturing, and some pressure was required to force water through the crack (see Figure 5). Breakdown pressure averaged 13 MPa, but was variable among several other test samples taken from the same block of Westerly granite.

The most striking self-potential observation during hydraulic fracturing was a large spike (both positive and negative) at the time of fracture initiation, up to 150 mV, persisting for ~10 msec. This can be seen in Figures 2 and 3, and corresponds to the observed time of failure from the pressure record. This SP response may be caused by electrokinetic coupling

as high-pressure injectate rushes into the newly created crack void space. The SP record also indicates that the pressure gradient driving this flow equilibrates quickly, as the transient SP decays rapidly. This is expected owing to the small sample size, the lack of confining pressure, and the observation that the induced fracture broke through to the sample edge.

Figure 2 shows the SP and pressure record for the ‘fresh’ (unaltered) Westerly granite core (WG1). Prior to failure the SP record is nearly invariant, suggesting little to no fluid infiltration during this time. This is not unexpected as the permeability of fresh Westerly granite is around $3 \times 10^{-19} \text{ m}^2$ (300 nd) [18]. Figure 3 shows the SP and pressure records for sample WG2. Prior to testing, this sample had been subjected to cycles of heating and rapid cooling to produce a system of micro-cracks altering the bulk permeability. The SP record for sample WG2 shows an increasing trend prior to fracture, indicating significant fluid infiltration. This flow likely results from both elastic and inelastic opening of micro-cracks and increased permeability with increasing pore pressure [19, 20].

Notably, there is little reduction in the breakdown pressure for the altered granite specimen compared to the fresh specimen (Figures 1 and 2). A lower breakdown pressure might be expected owing to the network of micro-cracks created by heating and quenching, and resulting poroelastic effects. However, we have not yet tested a sufficient number of samples to accurately quantify the breakdown pressure, and we have observed significant variation among our test samples, some of which failed at as low as 6.5 MPa.

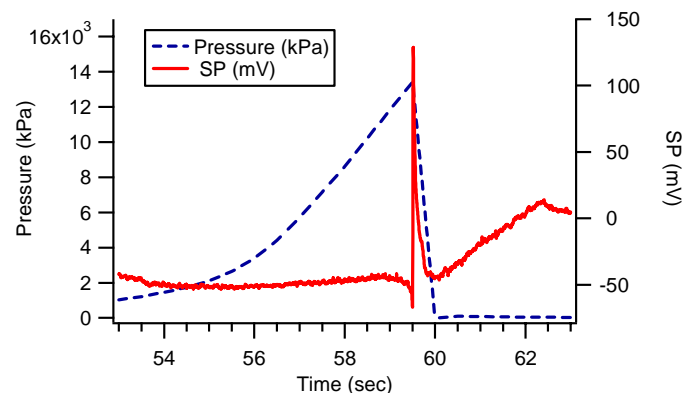


Fig. 2: SP and pressure records from a hydraulic fracture induced in *fresh* Westerly granite (sample WG1 – center electrode). The SP record indicates little to no fluid infiltration prior to sample failure.

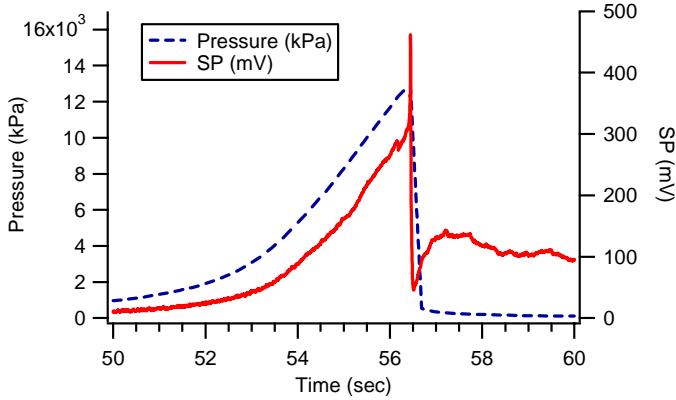


Fig. 3: SP and pressure records from a hydraulic fracture induced in *altered* westerly granite (sample WG2 – center electrode). This sample was pre-treated with 9 cycles of heating and quenching to produce a system of micro-cracks. Under increasing pore pressure these cracks dilated resulting in increased permeability, flow, and an increasing SP trend.

The SP spikes at failure occurred at different times at each electrode. In Figure 4 the SP records from all 3 electrodes are shown during a small interval of time surrounding failure of sample WG2. The timing of the SP spikes recorded by each electrode indicates the progression of local failure, where the SP response is greatest for the electrode nearest active cracking. For this test, we can resolve that failure occurred first near electrode SP3 (near the bottom of the sample) and progressed toward electrode SP1 (near the top of the sample). We were able to resolve fracture propagation direction consistently in our testing on 50 mm core samples, likely owing to the general proximity of the electrodes to the fracture.

The SP response also indicates that fracturing was episodic, as shown in Figure 4, where discrete SP spikes occur at different times. Episodic hydraulic fracture growth is commonly observed in both the field and laboratory [21]. Since the electrical response is instantaneous, we know the exact time of local fracturing. We also observed each individual SP event simultaneously on all 3 SP electrodes (Figure 4). For example, the primary failure event noted by electrode SP3 occurs at 56.438 sec and there are simultaneous, but subdued, SP spikes recorded by electrodes SP2 and SP1. The subdued response for these electrodes results from increased distance from the source, and indicates that each failure event was recorded throughout the system, with the largest response occurring at the electrode nearest the active crack tip.

Following the failure event, we flowed injectate through the fractured samples and observed that the

SP response for flow through an existing crack more closely mimicked the pressure record for increasing pressures (Figure 5), as predicted by electrokinetic theory (Eq. 6). However, we observed a slow decay of the SP following the end of injection, which may result from long hydraulic relaxation times and continued fluid circulation [9, 13].

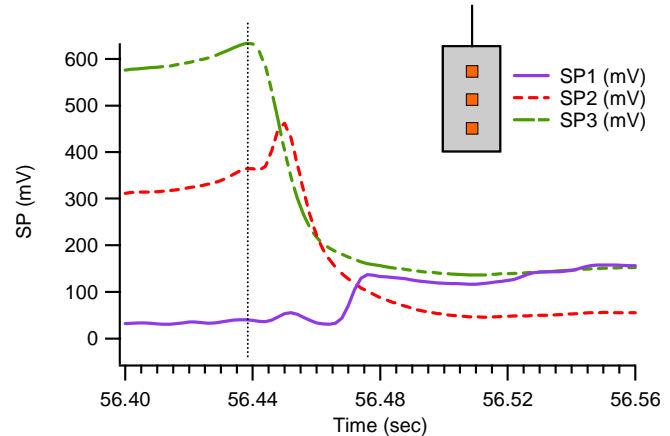


Fig. 4: Hydraulic fracture in altered Westerly granite (sample WG2). The time lag in SP spikes for electrodes SP1, SP2, SP3 indicates fracture propagation from electrode SP3 to SP1, or the bottom to top of the sample (see inset schematic), and a vertical crack propagation velocity of 1.34 m/s.

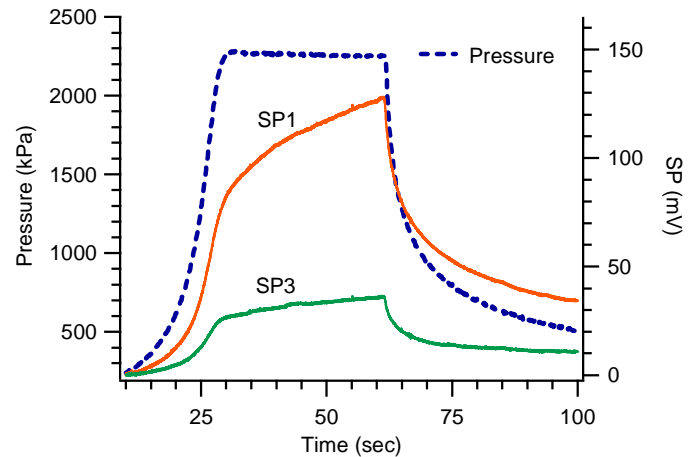


Fig. 5: Flow through an open fracture, and the corresponding pressure and SP response (sample WG2).

5. DISCUSSION

This testing revealed a distinct SP spike at the time of hydraulic fracture initiation, likely a result of electrokinetic coupling, as injectate rushed into the newly created fracture void space. Our samples broke through immediately and were not confined, so the pressure declined almost instantaneously. This is similarly represented in the SP response.

The effect of micro-cracks on the sample permeability is clearly indicated by comparing Figures 1 and 2. In Figure 1, the SP record for the fresh specimen is nearly invariant prior to fracture initiation, indicating little fluid infiltration. However, in Figure 2, the positive SP trend for the micro-cracked sample indicates significant flow prior to failure. Thus, by employing self-potential monitoring, information about fluid infiltration is obtained that is otherwise not apparent from the injection pressure data.

Following the initial failure event, the SP records for each electrode are less predictable, deviating from the trend of the injection pressure. This is likely a result of changes in moisture content around the electrodes as injectate expelled from the fracture hits the copper pads or runs down the sample wall. Wetting an electrode rapidly changes its contact resistance, similar to watering an electrode in the field [22]. Thus, little meaningful information about flow through the specimen was captured after the initial failure event.

There was some concern about whether water flowing in the steel injection tubing could itself create a streaming potential. In oil refineries, electrostatic discharges have reportedly caused a number of explosions as a result of electrokinetic coupling in non-aqueous solutions [23]. To test if our injection system generated a streaming potential we placed 2 electrodes 230 mm apart on a 6.35 mm diameter stainless steel tube, similar to that used in testing. A valve on the end of the tube allowed us to pressurize the water inside to 12 MPa. We then opened the valve to allow water to flow out and monitored any induced voltage across the electrode pair. We observed no voltage change created by water rushing through the steel tube.

The precise time of hydraulic fracture initiation was resolved from the SP time series. This is useful when employing other monitoring methods like acoustic emissions, where the speed at which the acoustic wave travels in the medium (which may be heterogeneous) must be known in order to determine the time of fracture initiation. With SP monitoring, the electric signal moves at the speed of light regardless of heterogeneity, so the exact time of fracture initiation can be determined from raw data.

Combining the SP time series from each electrode also enabled us to determine the direction of

fracture propagation. Fracture growth was episodic, as indicated by multiple discrete SP spikes, and the magnitude of the spikes differed for the various electrodes depending on their proximity to the active crack tip. Future work on larger samples will investigate the ability of SP measurements to provide information about fracture orientation and growth.

6. CONCLUSION

We have investigated the self-potential response during hydraulic fracturing by conducting a series of short experiments in the laboratory. We fractured cylindrical cores of Westerly granite by applying water at a constant rate to each sample center. Electrodes on the perimeter monitored the spatial and temporal SP response, which was marked by a distinct spike of up to 150 mV at the time of fracture initiation. This spike likely results from electrokinetic coupling as injectate rapidly moves into the fracture void space. One of the test specimens (WG2) was subjected to cycles of heating and quenching to produce a system of micro-cracks throughout the sample lattice. Under increasing pore pressure conditions these micro-cracks dilated leading to fluid infiltration, which was indicated by an increasingly positive SP trend. Finally, temporal resolution of the SP signals indicated the exact time of fracture initiation for the area nearest each electrode, and allowed us to reconstruct the direction of fracture propagation.

REFERENCES

1. Jouniaux, L., and J. Pozzi. 1995. Streaming potential and permeability of saturated sandstones under triaxial stress: consequences for electrotelluric anomalies prior to earthquakes, *J. Geophys. Res.*, 100(B6), 10,197-10,209.
2. Lorne, B., F. Perrier, and J. Avouac. 1999. Streaming potential measurements 1. Properties of the electric double layer, *J. Geophys. Res.*, 104(B8), 17,857-17,877.
3. Yoshida, S. 2001. Convection current generated prior to rupture in saturated rocks, *J. Geophys. Res.*, 106(B2), 2103-2120.
4. Wang, C., P. Sundaram, and R. Goodman. 1978. Electrical resistivity changes in rocks during frictional sliding and fracture, *Pure App. Geophys.*, 116, 717-731.
5. Chen, G., and Y. Lin. 2004. Stress-strain-electrical resistance effects and associated state equations for uniaxial rock compression, *Int. Journ. Rock Mech. Min. Sci.*, 41, 223-236.

6. Scholz, C., L. Sykes, and Y. Aggarwal. 1973. Earthquake prediction: A physical basis, *Science*, 181, 803-810.
7. Mizutani, H., T. Ishido, T. Yokokura, and S. Ohnishi. 1976. Electrokinetic phenomena associated with the Matsushiro earthquakes, *Geophys. Res. Lett.*, 3, 364-368.
8. Yoshida, S., O. Clint, and P. Sammonds. 1998. Electric potential changes prior to shear fracture in dry and saturated rocks, *Geophys. Res. Lett.*, 25, 1577-1580.
9. Wurmstich, B. 1995. 3D self-consistent modeling of streaming potential responses; theory and feasibility of applications in earth sciences, Doctoral Thesis, Texas A&M University, College Station, TX, United States.
10. Wurmstich, B. 1995. Feasibility of streaming potential measurements during hydrofracturing, *SEG Annual Meeting Expanded Technical Program*, 65, 30-32.
11. Revil, A., G. Saracco, and P. Labazuy. 2003. The volcano-electric effect, *J. Geophys. Res.*, 108(B5), doi:10.1029/2002JB001835.
12. Kawakami, N., and S. Takasugi. 1994. SP Monitoring during hydraulic fracturing using the TG-2 well, *European Association of Exploration Geophysicists; 56th meeting and technical exhibition, Vienna, Austria*.
13. Marquis, G., M. Darnet, P. Sailhac, and A. K. Singh. 2002. Surface electric variations induced by deep hydraulic stimulation: An example from the Soultz HDR site, *Geophys. Res. Lett.*, 29(14).
14. Pride, S. 1994. Governing equations for the coupled electromagnetics and acoustics of porous media, *Phys. Rev. B*, 50(21), 15,678-15,696.
15. Onsager, L. 1931. Reciprocal relations in irreversible processes, 1, *Phys. Rev.* 37, 405-426.
16. von Smoluchowski, M. 1903. Contribution à la théorie de l'endosmose électrique et de quelques phénomènes corrélatifs, *Bulletin International de l'Académie des Sciences de Cracovie*, 8, 182-200.
17. Zoback, M. D., and Byerlee, J. D. 1975. The effect of microcrack dilatancy on the permeability of Westerly granite, *J. Geophys. Res.*, 80(5), 752-755.
18. Brace, W. F., J. B. Walsh, and W. T. Frangos. 1968. Permeability of granite under high pressure, *J. Geophys. Res.* 73(6), 2225-2236.
19. Bernaix, J. 1969. New laboratory methods of studying the mechanical properties of rocks, *Int. Journ. Rock Mech. Min. Sci.*, 6, 43-90.
20. Simpson, G., Y. Guéguen, and F. Schneider. 2001. Permeability enhancement due to microcrack dilatancy in the damage regime, *J. Geophys. Res.*, 106(B3), 3999-4016.
21. Wills, P., D. DeMartini, H. Vinegar, J. Shlyapobersky, W. Deeg, J. Woerpels, J. Fix, G. Sorrells, and R. Adair. 1992. Active and passive imaging of hydraulic fractures: *The Leading Edge*, 11(7), 15-22.
22. Corwin, R. F., and D. B. Hoover. 1979. The self-potential method in geothermal exploration; *Geophysics*, 44(2), 226-245.
23. Morrison, I. D. 1993. Electrical charges in nonaqueous media, *Colloids and Surfaces A*, 71, 1-37.